HHS Public Access

Author manuscript

Nat Neurosci. Author manuscript; available in PMC 2013 October 01.

Published in final edited form as:

Nat Neurosci. 2013 April ; 16(4): 507–516. doi:10.1038/nn.3346.

Optical Control of Metabotropic Glutamate Receptors

Joshua Levitz[1], **Carlos Pantoja**[2], **Benjamin Gaub**[3], **Harald Janovjak**[2,4], **Andreas Reiner**[2], **Adam Hoagland**[2], **David Schoppik**[5], **Brian Kane**[6], **Philipp Stawski**[7], **Alexander F. Schier**[5], **Dirk Trauner**[6,7,#], and **Ehud Y. Isacoff**[1,2,3,8,#]

[1]Biophysics Graduate Group, University of California, Berkeley, CA, USA

[2]Department of Molecular and Cell Biology, University of California, Berkeley, CA, USA

[3]Helen Wills Neuroscience Graduate Program, University of California, Berkeley, CA, USA

[5]Harvard University, Dept. of Molecular and Cellular Biology, Cambridge MA

[6]Department of Chemistry, University of California, Berkeley, CA, USA

[7]Department of Chemistry and Center of Integrated Protein Science, University of Munich, Munich, Germany

[8]Physical Bioscience Division, Lawrence Berkeley National Laboratory, Berkeley, California, USA

Abstract

G-protein coupled receptors (GPCRs), the largest family of membrane signaling proteins, respond to neurotransmitters, hormones and small environmental molecules. The neuronal function of many GPCRs has been difficult to resolve because of an inability to gate them with subtype-specificity, spatial precision, speed and reversibility. To address this, we developed an approach for opto-chemical engineering native GPCRs. We applied this to the metabotropic glutamate receptors (mGluRs) to generate light-agonized and light-antagonized “LimGluRs”. The light-agonized “LimGluR2”, on which we focused, is fast, bistable, and supports multiple rounds of on/off switching. Light gates two of the primary neuronal functions of mGluR2: suppression of excitability and inhibition of neurotransmitter release. The light-antagonized “LimGluR2block” can be used to manipulate negative feedback of synaptically released glutamate on transmitter release. We generalize the optical control to two additional family members: mGluR3 and 6. The system works in rodent brain slice and in zebrafish *in vivo*, where we find that mGluR2 modulates the threshold for escape behavior. These light-gated mGluRs pave the way for determining the roles of mGluRs in synaptic plasticity, memory and disease.

[#]Please address correspondence to dirk.trauner@lmu.de and ehud@berkeley.edu.

[4]Present address: Institute of Science and Technology Austria, Klosterneuburg, Austria

Author Contributions

J.L. designed experiments and conducted homology modeling, Monte Carlo simulations, HEK293 cell patch experiments, cAMP measurements, cultured neuron and hippocampal slice patch experiments, analyzed data, and wrote the manuscript. C.P.. designed zebrafish experiments, conducted zebrafish behavioral experiments, analyzed data, and wrote the manuscript. B.G. and A.R. conducted HEK293 cell patch experiments. H.J. designed and conducted Monte Carlo simulations. P.S. and B.K. synthesized photoswitches. A.H., D.S. and A.S. developed and setup zebrafish behavioral apparatus. D.T. developed photoswitching methodology and provided photoswitches. E.I. supervised the project, designed experiments, analyzed data, and wrote the manuscript.

Introduction

Optogenetics has revolutionized neuroscience by making it possible to use heterologously expressed light-gated ion channels and pumps to stimulate or inhibit activity in genetically selected neurons and brain regions and thereby determine their roles in circuit function and behavior[1,2]. Since the flow of information through neural circuits depends on the strength of synaptic transmission and changes in synaptic strength are critical to neural processing as well as learning and memory, an important further development would be to bring optogenetics to the native pre- and postsynaptic receptors that control synaptic transmission and plasticity.

Of special interest are G-protein coupled receptors (GPCRs), the largest class of membrane signaling proteins, which, because of their importance to disease, are the most explored drug targets in all of biology. GPCRs respond to a wide-array of stimuli and contain a seven transmembrane domain that couples to heterotrimeric G-proteins, including the G_q, G_s, G_t, and $G_{i/o}$ families through which they regulate a variety of other signaling proteins[3]. Recent X-ray structures have increased our understanding of how GPCRs interact with external ligands and couple intracellularly with G-proteins[4]. Despite these efforts there remains a paucity of selective pharmacological tools for GPCRs and the specific biochemical, physiological, and behavioral roles of many GPCRs are not well-understood. In neural systems, GPCRs are found mostly on sensory cilia and at synapses. The same GPCR may be found on both presynaptic excitatory and inhibitory nerve terminals, as well as on dendritic spines and associated glial processes[5], making it difficult to determine its specific function in each compartment, and leaving undefined the mechanism of induction of synaptic plasticity. Even though multiple GPCRs in a cell may couple to the same G-proteins they often activate distinct targets due to molecular interactions that co-localize them in specific protein complexes which can lead to unique patterns of regulation[3,6,7].

Thus, to determine the function of a GPCR one needs specific tools for subtype-selective, cell-type specific, spatially precise and, ideally, rapid and reversible manipulation. The ability to engineer individual full-length GPCRs to be activated or blocked by remote control could provide a general solution for these problems. GPCRs have already been engineered to respond to non-native ligands—the so-called RASSLs and DREADDs—and used to orthogonally activate G protein pathways *in vitro*[8] and *in vivo*[9]. Because these receptors lack the spatiotemporal precision of optical manipulation, interest has remained in the development of light-activated GPCRs. Until the present, the effort has centered on the naturally light-sensitive rhodopsin[10–14] and melanopsin[15–17] and chimeras that combine the transmembrane portions of rhodopsin with the cytoplasmic loops of adrenergic or serotonergic receptors that couple to other G-proteins[18–20]. While these foreign or chimeric receptors can be used to activate specific G proteins, they lack signaling specificity because they lack the complete sequence (and thus normal protein interactions) of the native GPCR. Moreover, since they require 11-*cis* retinal as a photoswitch, which is lost following photoisomerization, they cannot trigger either sustained or reproducible signals because of incomplete recovery following photo-stimulation[21].

We have solved these problems by developing an optochemical method for controlling native mammalian GCPRs with light. We employed synthetic photoswitchable tethered ligands (PTLs) that could be targeted to genetically modified versions of native receptors[1,22], as done earlier to light-block K^+ channels[23] and light-activate the ionotropic kainate receptor[24]. We targeted the eight-member metabotropic glutamate receptor (mGluR) family. mGluRs are class C GPCRs that are allosterically regulated by glutamate binding to a large extracellular clamshell ligand binding domain (LBD)[5]. mGluRs respond to spatially confined, temporal patterns of synaptic and extrasynaptic glutamate to regulate neuronal excitability, transmitter release, and synaptic plasticity[5,25,26]. They include presynaptic receptors, which provide feedback control over glutamate release from excitatory nerve terminals as well as control of GABA release from inhibitory nerve terminals, postsynaptic receptors that modulate synaptic signaling in dendritic spines and receptors in astrocytic processes that are intimately associated with synapses and respond to neuronal activity in several ways, including by the release of gliotransmitters[27,28]. The mGluRs are divided into three groups[5]. We focused on the group II mGluRs, mGluR2 and 3, which couple to the $G_{i/o}$ pathway to inhibit adenylyl cyclase[29], activate GIRK channels to reduce excitability and inhibit presynaptic voltage-gated calcium channels to inhibit neurotransmitter release[30,31]. These mGluRs operate in synaptic plasticity in multiple brain regions[25,26], participate in fundamental behavioral processes, including memory[32], and represent major drug targets for neuropsychiatric disorders[33]. We extended our engineering to the Group III mGluR, mGluR6, which also couples to $G_{i/o}$, but has distinct expression patterns, subcellular targeting and regulation and, as a consequence, distinct roles in brain circuits[5].

A combination of structural analysis and synthesis of novel compounds was used to develop new PTLs with maleimide at one end for cysteine attachment, a photoisomerizable azobenzene linker and glutamate as the ligand at the other end. Monte Carlo simulations enabled us to determine PTL attachment points such that photoisomerization of the azobenzene would toggle the PTL from a conformation that permits glutamate binding to one that does not. The approach was successful for both photo-agonism and photo-antagonism of mGluR2. Light rapidly, reversibly and reproducibly turns mGluR2 on and off. The photo-control is bistable and can be used to toggle excitability and pre-synaptic inhibition in cultured neurons and brain slices. *In vivo*, mGluR2 photo-agonism can be used to reversibly and repeatedly modulate escape behavior in larval zebrafish, a fast control of a previously unknown native form of regulation of the acoustic startle response (ASR). The photo-control approach is generalizable: we have transferred it to mGluR3 and mGluR6. The introduction of photosensitivity into native GPCRs provides the means for probing their biological functions at a level of precision not previously available.

Results

Tether Model Pharmacology and Monte Carlo Simulations

To design photocontrol of mGluR2 we built a homology model of the mGluR2 LBD based on the mGluR3 crystal structure[34] (Fig. S1a–c) and tested a series of test compounds, termed Tether Models (Fig. 1a), which demonstrated that, unlike the 4’L requirement at ionotropic glutamate receptors, 4’D stereochemistry is required for mGluR2 and that a short tether (i.e.

D-Tether-0) acts as an agonist, whereas a longer tether (i.e. D-Tether-1) acts as an antagonist (Fig. S1;). This study provided the impetus for synthesizing D-MAG-0 and D-MAG-1 (Fig. 1b) with the goal of identifying attachment points for optical agonism (Fig. 1c) or antagonism (Fig. 1d).

In order to rationally design light-gated versions of mGluR2, we used Monte Carlo simulations to identify geometrically appropriate cysteine-attachment points for the conjugation of D-MAG-0. First, we built a homology model of mGluR2 in the open, glutamate-bound state using the mGluR1 open, glutamate-bound crystal structure (PDB ID: 1EWK) as a template. We then generated molecular models of D-MAG-0 with geometries of *cis*- and *trans*- azobenzene based on earlier experimentally determined coordinates that were validated computationally[35]. After manually positioning the glutamate-group of D-MAG-0 in the binding pocket, the Monte-Carlo multiple minimum (MCMM) algorithm[36] was used to search the space accessible to D-MAG-0 with single-bond rotations as degrees of freedom. Twenty thousand orientations/structures were generated by MCMM and for each the distance from the cysteine-reactive maleimide (Mal) group of MAG to every residue on the surface of the LBD was measured automatically. Simulations were performed for both *cis* and *trans* conformations of D-MAG-0 (Fig. 2a). The conformational search identified eight clusters of 3–8 residues that were significantly populated by the Mal-group of D-MAG-0 (Fig. 2b).

Based on the Monte Carlo simulations, we selected a subset of seven residues with orientations favorable for the maleimide end of MAG to conjugate and for its glutamate end to enter the ligand-binding site without steric clashes. Seven candidate sites were identified: Q42, D146, E373 and S376 in the upper lobe of the LBD, L300 and S302 on the lower lobe, and D215 at the hinge (Fig. 2c). Each site was individually substituted with cysteine and co-expressed with GIRK1 in HEK293 cells.

Photo-Antagonism by D-MAG-1: LimGluR2-block

We focused initially on two MAG attachment sites, L300C and S302C, because of their high scores in the Monte Carlo simulations and their large photo-effects (Fig. 2b, Supplementary Table 1). Cells expressing either variant along with GIRK1, were labeled with either D-MAG-0 or D-MAG-1 (50–100 μM) for 30–60 minutes, patch-clamped in the whole cell configuration and alternately challenged with 380 nm light to isomerize the photoswitch to *cis* and 500 nm light to isomerize to *trans*. This was done in the absence of glutamate to determine if there was photo-agonism or in the presence of glutamate to determine if there was photo-antagonism. Importantly, no photoeffects were observed in cells expressing wild-type mGluR2 and labeled with D-MAG-0 or D-MAG-1 (Supplementary Table 1).

Following labeling at S302C and L300C with D-MAG-1 we found that illumination at 380 and 500 nm had no effect on the current (Fig. 3a, S2a). However, in the presence of glutamate, 380 nm light induced a marked decrease in the current that was reversed by illumination at 500 nm (Fig. 3a, S2a). Repeated switching between 380 and 500 nm light toggled the glutamate-induced current between high and low levels. The percentage photo-antagonism was 21 ±2% (n = 7) for D-MAG-1 at L300C and 53 ± 4% (n = 5) at S302C in 1 mM glutamate. At concentrations greater than 1mM, photoantagonism was decreased (Fig.

S2b,c), indicating a competitive mechanism. D-MAG-1 antagonism is consistent with the antagonism of the D-Tether-1 compound, observed above. Due to the large potency of the 302C substitution in combination with D-MAG-1, we term this tool “LimGluR2-block”.

An advantageous property of the azobenzene photoswitches used here is their thermal bistability, which makes it possible to produce persistent occupancy in the dark of the *cis* state following a photo-isomerizing light pulse[37,38]. Indeed, we found that brief light pulses at 380 nm induced antagonism that was stable in the dark until it was reversed by 500 nm illumination (Fig. 3b).

Photo-Agonism by D-MAG-0: LimGluR2

We next turned to the version of MAG that was based on the agonist D-Tether-0: D-MAG-0. We focused on the L300C/D-MAG-0 combination because of the utility of photo-activation, and refer to it henceforth as “LimGluR2”. The photo-activation of LimGluR2 by 380 nm light yielded currents about half as large as those evoked by saturating glutamate (48 ± 4% compared to 1 mM glutamate, n=10) (Fig. 3c). Illumination at 500 nm rapidly terminated the activation of the GIRK1 channels (Fig. 3c–f). Voltage ramps confirmed that the light-activation of LimGluR2 at 380 nm was due to the opening of the same inward-rectifying potassium conductance as was activated by glutamate (Fig. S3a).

Notably, no antagonism of the glutamate response was induced by illumination at 380 nm (Fig. 3c, S3c). This suggests that the lack of full activation by D-MAG-0 attached to L300C is not due to partial agonism by *cis*-D-MAG-0. Application of glutamate following illumination at 380 nm increased the inward current above the level induced by light alone (Fig. S3b). This result further indicates that MAG does not lock the LBD in a partially-active conformation, but rather functions as a full agonist in a fraction of subunits. LimGluR2 maintained close to normal affinity for glutamate (Fig. S3d) and retained the ability to be activated or antagonized by standard group II mGluR pharmacological agents (Fig. S3e, f)

As with the bistability of LimGluR2block, we found that brief activating light pulses at 380 nm evoked a period of GIRK activation that persisted for tens of seconds in the dark, and which could be rapidly turned off by illumination with 500 nm light (Fig. 3d). During this bout of protracted activation in the dark the current declined by ~10–20%, a decline that was similar to what was seen under continuous illumination of LimGluR2 at 380 nm, as well as in response to extended application of glutamate (Fig. 3a; Fig. S4a). At moderate light intensities (10–20 mw/mm^2) bistable activation and deactivation were elicited by brief light pulses (250 ms pulse at 380 nm to activate and 1 s pulse at 500 nm to deactivate) of LimGluR2 induced GIRK currents with identical amplitude and kinetics to currents induced by extended illumination (Fig. S4a–c). At higher light intensities (~40 W/mm^2), signaling could be activated by sub-millisecond pulses of light (Fig. 3e), indicating that these brief pulses are sufficient to ligand the receptor and that the kinetics of effector activation and deactivation are rate-limited by subsequent signaling steps.

Repeated bouts of photoswitching of LimGluR2 yielded multiple rounds of photo-activation of GIRK1 channels without decline of the response (Fig. 3f), consistent with the lack of

GRK-dependent desensitization of mGluR2[39,40]. Having observed the reproducibility of LimGluR2, we asked how it compares with the earlier light-gated GPCRs that are made either of rhodopsin or of rhodopsin chimeras. To address this, we tested the critical light-gated component of all of the prior GPCRs: rhodopsin. Rat rhodopsin, RO4, which also couples to GIRK1 channels[13], was expressed in HEK293 cells and the cells were incubated for 40 minutes in 1 uM 11-cis retinal in the dark. Illumination of cells co-expressing RO4 and GIRK1 with 490 nm light activated large inward GIRK currents (Fig. S5a) that were similar in amplitude and rise time to those evoked by LimGluR2 (Fig. S5b). However, the GIRK1 deactivation speed of RO4 upon light turn-off was much slower than upon light-driven deactivation of LimGluR2 (Fig. S5a–c). Due to the slow deactivation kinetics of RO4, repeated optical stimulation was limited to intervals of 90 s (Fig. S5d). Even at this long interval the RO4-mediated responses declined significantly from pulse to pulse (Fig. S5d,f). In contrast, LimGluR2 photo-responses were stable in amplitude (Fig. 3d, S5e, f).

Having seen that LimGluR2 can photo-activate $G_{\beta\gamma}$-mediated signaling, as assayed with GIRK currents, we asked if it could also photo-activate G_{α}-mediated signaling by measuring its ability to reduce cellular cAMP levels. When labeled with D-MAG-0 and stimulated with 380 nm light, LimGluR2 reduced the elevation of cAMP that is triggered by forskolin with an efficacy approaching that of 1 mM glutamate (Fig. 3g). This indicates that *cis*-D-MAG-0 activates mGluR2 in the same way as glutamate to induce native downstream signaling.

Generalization of Photocontrol to mGluR3 and mGluR6

To test if the PTL approach could be generalized to other mGluRs, we tested cysteine substitutions in mGluR3, the other group II mGluR member, and mGluR6, a group III mGluR member, at residues that are homologous to L300 of mGluR2 (Fig 4a). Optical control of mGluR3 is attractive because of the lack of agonists and antagonists that differentiate between mGluR2 and 3 except for a recently described compound that agonizes mGluR2 and antagonizes mGluR3[41]. mGluR6 is an important target for photocontrol because of its central role in synaptic transmission from photoreceptors to ON bipolar cells in the retina.

Conjugation of mGluR3 Q306C with D-MAG-0 produced strong photo-agonism (“LimGluR3”) under 380 nm light (Fig. 4b). The photocurrents were 74 ± 12 % (n= 6 cells) the amplitude of 1 mM glutamate evoked currents, indicating that LimGluR3 is even more efficient than LimGluR2. Conjugation of mGluR6-K306C with D-MAG-0 produced a strong photo-antagonism under 380 nm light (Fig. 4c). The percentage photo-antagonism was 40 ± 3 % (n =5 cells; 1 mM glutamate) for D-MAG-0 at mGluR6-K306C. We term this tool “LimGluR6-block”. Notably, photoswitching of D-MAG-0 anchored at sites of mGluR3 and mGluR6 that are homologous to mGluR2’s L300 yielded similar photo-agonism in mGluR3 but photo-antagonism in mGluR6, providing a readout of the degree of geometric similarity near the LBD binding pocket.

Optical Control of Excitability in Hippocampal Neurons

In addition to the functional advantages over existing photoswitchable GPCRs, LimGluR2 is a native receptor that could make it possible to optically stimulate native mGluR2 targets

with light. To test this, we examined the ability of LimGluR2 to optically modulate native downstream targets of mGluR2 in cultured hippocampal neurons. These targets include somatodendritic GIRK channels[42] and voltage-gated calcium channels in the presynaptic nerve terminal[43,44], both of which should be within reach of mGluR2-L300C, which we found to distribute to the soma and many fine processes (Fig. 5b).

We first tested the expectation that activation by LimGluR2 of cell body GIRK channels would decrease excitability (Fig. 5a). In high extracellular potassium (60 mM) and under voltage clamp, illumination with 380 nm light evoked large inward currents that were deactivated by 500 nm light (Fig. S6a). With illumination at a fixed intensity (0.4 mW/mm^2 at 380 nm), photo-activation was ~5-fold faster in neurons than in HEK293 cells (respectively, the single exponential fits were: τ=1.03±0.06 s, n=5, *versus* 5.69 ±0.69, n=8; unpaired, 1-tailed t-test, p=0.004). This is consistent with previous observations of faster activation of GIRK channels by native GPCRs in cultured neurons compared to heterologously expressed receptors in GIRK-transfected HEK293 cells[45] and suggests that LimGluR2 integrates into the native G-protein signaling machinery of neurons.

To test the ability of LimGluR2 to modulate neuronal excitability via GIRK channel activation, we performed current clamp experiments. Neurons expressing LimGluR2 were labeled with D-MAG-0 and given depolarizing current injections, in 10 pA increments, under current clamp. This was done during alternating illumination with 380 nm and 500 nm light. Photo-activation of LimGluR2 at 380 nm decreased the number of action potentials fired evoked by each level of depolarization (Fig. 5c, d). This optical inhibition was highly reversible and repeatable (Fig. 5c, e, f; Fig S5B). The photo-currents were large enough to evoke a reversible 3–10 mV hyperpolarization at the resting potential (Fig. 5e) and, in accordance with the bistability of the system, the hyperpolarization and silencing persisted for tens of seconds in the dark after activation of LimGluR2 by a brief 380 nm light pulse (Fig. 5e).

Optical Control of Synaptic Transmission

Group II metabotropic glutamate receptors are known to traffic to presynaptic terminals and play inhibitory roles in synaptic transmission and plasticity[5,25]. We asked whether LimGluR2 would provide for optical control of neurotransmitter release (Fig. 6A). We expressed mGluR2-L300C in low-density hippocampal cultures in which each neuron forms synapses onto itself (autapses). Cells were patch-clamped we recorded postsynaptic currents elicited by brief depolarization steps that elicited single action potentials. Excitatory post-synaptic currents (EPSCs) were detected in some cells (Fig. 6b) and inhibitory post-synaptic currents (IPSCs) were detected in others (Fig. 6c). Activation of LimGluR2 by 380 nm light rapidly and reversibly inhibited both the EPSCs (41±5%, n =8) and IPSCs (36 ± 3%, n =4) (Fig. 6b and c).

In contrast to the potent inhibition by LimGluR2, there was no optical inhibition in either cells transfected with GFP instead of LimGluR2 or cells transfected with LimGluR2 but not labeled with D-MAG-0 (Fig. 6d). Moreover, there was no change in baseline PSC amplitude in labeled and transfected (LimGluR2) cells compared to GFP-transfected or unlabeled cells (223±64 pA; n=12 vs. 262± 68 pA; n=5 vs. 232±91 pA; n=5). In addition, the optical

inhibition of transmission by LimGluR2 produced no change in PSC decay time (Fig. S7a), time to peak (Fig. S7b) or jitter (S.E.M of time to peak), leaving the post-synaptic currents unchanged in shape (Fig. S7c).

To test if the LimGluR2-mediated optical inhibition of transmission proceeds through a pre-synaptic mechanism, we performed paired pulse experiments. The optical inhibition of transmission by illumination with 380 nm light was associated with a significant increase in the relative size of the EPSC evoked by the second pulse (Fig. 6e, f, g; paired, 1-tailed t test, p=0.01). Similarly, during high frequency (25 Hz) stimulation of autapses 380 nm light increased short-term facilitation relative to during 500 nm light (Fig. S7d–f). This indicates that activation of LimGluR2 inhibits postsynaptic currents by decreasing release probability and, thereby, increasing facilitation. This is exactly the mechanism by which native mGluR2 acts presynaptically via inhibition of N and P/Q type voltage-gated calcium channels, as has been observed for native group II mGluRs at the calyx of Held[43].. The paired pulse ratio in LimGluR2 positive cells was the same as that in GFP-transfected cells (respectively 1.5±0.1, n=5 vs. 1.4± 0.3, n=4), indicating that expression and labeling of LimGluR2 does not alter basal release.

Finally, we tested the ability of LimGluR2 to produce multiple rounds of inhibition of transmission and recovery and for the inhibition to outlast the activating light pulse due to the bistable nature of the photoswitch. Brief photo-activation produced sustained inhibition of synaptic transmission that persisted in the dark for minutes and could be rapidly reversed by illumination at 500 nm (Fig. 6h; Fig. S7g).These experiments show that LimGluR2 provides a means for the reversible, repeatable optical control of presynaptic inhibition of neurotransmitter release.

Optical Control of Tonic Inhibition by LimGluR2-Block

We next assessed the ability of photoantagonism by LimGluR2-Block to modulate receptor function in neurons in response to native glutamate. We tested if photo-antagonism by “LimGluR2-block” could alter spike-firing patterns in cultured hippocampal neurons. In regions with high transfection efficiency (>1 transfected neuron per field of view) optical antagonism of mGluR2 with 380 nm light resulted in an increased firing frequency that was reversed by 500 nm light (Fig. S8a, b). This experiment demonstrates that LimGluR2-block is robust enough to alter neuronal signaling properties despite incomplete antagonism. Furthermore, this indicates that under basal conditions there is sufficient inhibitory tone produced by glutamate binding to mGluR2 to suppress spike firing.

We also tested LimGluR2-block in autaptic neurons. Under basal stimulation frequencies (0.1 Hz) photo-antagonism of mGluR2 induced an increase in EPSC amplitude (Fig. (S8c,d; average increase in amplitude= 26 ± 8 %; n= 6 cells). This result is consistent with the observation that photo-antagonism of mGluR2 leads to an increase in spike firing frequency and indicates that glutamate feedback at excitatory nerve terminals can provide inhibitory tone via mGluR2, even within a sparsely-connected network. In contrast, at inhibitory autapses LimGluR2block did not induce a change in IPSC amplitude (Fig. S8e, f; average increase in amplitude=1.0± 0.02 %; n= 3 cells), suggesting that inhibition of transmitter release *via* mGluR2 under sparse activity operates by local signaling at individual excitatory

synapses, and that cross talk to inhibitory synapses may require high frequency coordinate activity and global glutamate spillover.

Optical Control of Excitability in Hippocampal Slices

We tested LimGluR2 in organotypic hippocampal slices prepared from P6–P8 rats co-transfected with td-Tomato as a transfection marker. Slices were incubated with D-MAG-0 and whole cell patch-clamp recordings were performed on cells up to two or three layers below the surface of the slice. At resting potential (−45 mV to −65 mV) LimGluR2 activation by illumination at 390 nm induced a 3–8 mV, reversible hyperpolarization (Fig. 7a). In response to depolarizing current injections, illumination at 390 nm reproducibly decreased action potential firing (Fig. 7b, c), as was seen in the dissociated cultured neurons (Fig. 5c, d). Illumination with 500 nm light restored firing frequency to levels seen before LimGluR2 activation. In addition, LimGluR2 activation was able to decrease spontaneous spike firing (Fig. 7d) in a bistable, reversible and reproducible manner. Importantly, LimGluR2 expression and D-MAG-0 labeling did not adversely affect neurons, leaving the average resting membrane potential unaltered (Fig. S9a). Also, no photo-effects were observed with D-MAG-0 in the absence of mGluR2-300C (S9b, d) or with mGluR2-300C but in absence of D-MAG-0 (S9c), indicating that orthogonality is maintained in slices. These results indicate that expression, labeling, and optical activation of LimGluR2 are attainable in intact tissue, providing a powerful means to probe the role of G-protein signaling in general, and mGluRs in particular, in the native preparation. We next turned to *in vivo* experiments to determine if LimGluR2 activation in neurons could alter behavior.

Optical Control of Zebrafish Behavior

To determine if LimGluR2 could be used *in vivo* to probe mGluR signaling in a behavioral context, we turned to the ASR of zebrafish (*Danio Rerio*), a well-characterized behavior of teleosts that is similar to the mammalian startle response[46].

At 5–6 dpf, fish were individually mounted in a glass-well petri dish with the head embedded in agar and subjected to sound/vibration stimuli (900 Hz, 120 ms) ranging from low energy to high energy (0.1mVpp-10mVpp, 0.5mVpp increments). At lower energy levels the sound/vibration stimulus induced forward swims, while higher energy levels elicited escape responses with the typical C-bend[47]. We found that wild-type (WT) fish treated with the non-specific group II mGluR agonist L-CCG-1 displayed a significantly decreased threshold of the ASR when compared to vehicle treated fish (Mann–Whitney, $n_{ct} = n_{LCCG-1} = 78$, $P < 0.02$, two-tailed) (Fig. 8a). This result indicates that activation of native group II mGluRs leads to a decrease in the threshold of the ASR in wild-type zebrafish.

Next, we tested if optical activation of LimGluR2 could recapitulate the native group II mGluR signaling effect of decreasing the threshold of the zebrafish ASR. First, we generated transgenic zebrafish in which LimGluR2(L300C) expression is driven by repeats of the GAL4 Upstream Activating Sequence (UAS). We crossed these *UAS:LimGluR2* zebrafish to *elavl3:Gal4;UAS:Kaede* fish to generate elavl3:Gal4;UAS:Kaede;UAS:LimGluR2 zebrafish. The *elavl3* promoter (also known as HuC) drives pan-neuronal expression of Gal4 and consequently of LimGluR2, as well as of

the Kaede fluorescent protein, which served as a marker for the *elavl3:Gal4* transgene (Fig. 8b). *elavl3:Gal4;UAS:Kaede;UAS:LimGluR2* zebrafish 5 days post-fertilization (dpf) were indistinguishable in swimming behavior (Fig. S10c–e) and ASR (Fig. S10f) from *elavl3:Gal4;UAS:Kaede fish*, which contained the neuronal driver alone. Fish health and responses to touch were unaffected by the 45 minute exposure to D-MAG-0 and 1 hour recovery. The ASR was also not significantly affected in a control transgenic line that does not express LimGluR2 and was treated with D-MAG-0 (Fig. S10g). These results demonstrate that neither pan-neuronal expression of LimGluR2 nor D-MAG-0 treatment modify health or behavior.

LimGluR2 was photo-controlled by patterned illumination applied caudal to the eyes in a region covering the cranial nerves, hindbrain and the rostral portion of the spinal circuits that control the escape response. To activate LimGluR2 we illuminated the fish with 380 nm light for 400ms and to deactivate it we applied 510 nm light for 1s. Activation of LimGluR2 increased the probability of an escape response (Fig. 8c, d). This effect was reversed by 510 nm light and could be toggled back and forth by repeatedly activating and deactivating LimGluR2 (Fig. 8c). The behavior of fish expressing LimGluR2 but not labeled with D-MAG-0 was not altered by light (Fig. 8d). In addition, labeling of fish with D-MAG-0 did not alter the basal threshold for the ASR (Fig. S10h). These results suggest a role for mGluR2 in the ASR and establish that LimGluR2 can be used to study mGluR2 signaling *in vivo*.

Discussion

GPCRs represent the largest family of membrane signaling proteins and respond to a wide-array of stimuli. These seven transmembrane receptors couple to distinct classes of heterotrimeric G-proteins, leading to the activation or inhibition of a large number of protein targets[3]. The diversity of signaling is vastly greater than can be accounted for by the four classes of G-proteins to which GPCRs couple. The additional diversity comes from several factors, including localization into specific subcellular compartments, corralling into signaling nanodomains with particular effectors, assembly of preformed GPCR-G protein-effector complexes, heteromultimerization into complexes with specialized properties, and unique profiles of interaction with regulatory proteins[6,7].

To elucidate GPCR function one needs a method that combines specific pharmacology with specificity for region, cell-type and subcellular compartment. At the same time one wants the approach to allow for the GPCR to be activated at physiological rates (i.e. the millisecond time scale) and to be reversible and reproducible to mimic physiological signaling and permit quantitative analysis. All this needs to be achieved on the full-length GPCR in order to maintain normal targeting and interaction with signaling partners and regulators. We overcame these obstacles by developing, via the rational design and synthesis of new PTLs called D-MAGs and a novel, simple and fast Monte Carlo simulation approach to select anchoring sites for these PTLs in order to generate photo-agonizing and photo-antagonizing versions of three of the eight mGluRs, representing two of the three mGluR groups. These approaches can readily be adapted to other target proteins and PTLs.

We most thoroughly characterized the photo-agonism with D-MAG-0 at position L300C of mGluR2 (LimGluR2). Unlike rhodopsin, which was the basis of most of the prior light-gated GPCRs, LimGluR2 can be actively toggled both on and off in less than one millisecond, enabling signaling to be controlled. on a synaptically-relevant timescale and providing for fast effector kinetics. Moreover, LimGluR2 permits repetitive stimulation at high rates without decline. Rhodopsin requires constant illumination to be activated, which increases the chance of tissue damage and can act as a confounding variable for behavioral studies, while LimGluR2 is bistable, eliminating the need for constant illumination. Most importantly, optical control of native GPCRs provides a unique opportunity to examine the specific synaptic and circuit functions of each receptor, which emerge from their restricted effector and regulatory profiles and cannot be deduced from widespread activation of the entire signaling pathway of the G-protein to which they couple.

We show that, despite their limited homology (66% identity between mGluR2 and mGluR3 and 44% identity between mGluR2 and mGluR6), photo-control can be generalized within the mGluR family from mGluR2 to the other Group II member mGluR3 and the Group III members mGluR6, with the same D stereoisomer linkage to the glutamate of MAG being required. Differences in photo-switching with a particular MAG at homologous sites of these three mGluRs reveals differences between their LBDs. This information may be useful for designing additional photoswitches or other pharmacological ligands as well as for probing the mechanism of clamshell closure.

The LimGluRs provide rapid, reversible, bistable, and highly reproducible control of excitability and synaptic transmission in dissociated cultured neurons as well as brain slice, two of the prime *in vitro* systems where synaptic transmission and plasticity in general, and mGluR function in particular, are studied most extensively. Although the photo-agonism and photo-antagonism of LimGluR2 are not complete, the photo-agonism induces characteristic mGluR2-dependent modulation and the photo-antagonism prevents the induction of such changes by native glutamate release. The precise temporal control, which allows the agonist or antagonist to be toggled on and off in a time-coupled manner, repeatedly and reproducibly makes it possible to observe small effects that would be difficult to distinguish with classical drugs. In the case of LimGluR2block, the photoeffect in neurons is consistent with the behavior of most neurotransmitter-gated GPCRs, which tend to be localized outside of the synaptic cleft and experience sub-saturating concentrations of the neurotransmitter. The success of the D-MAG labeling and photo-control of mGluRs in brain slice suggests that the approach should also work in the mammalian brain *in vivo*, as has been shown for a similar photoswitch directed to the ionotropic kainate receptor in the mouse retina i*n vivo*[48]. Indeed, we demonstrate that LimGluR2 works effectively *in vivo* in zebrafish when D-MAG is simply added to the zebrafish larvae E3 salt water medium.

We used LimGluR2 to photo-manipulate mGluR2 signaling in the context of the zebrafish ASR, a widely-studied behavior that is intriguingly similar in architecture and pharmacological regulation to the mammalian acoustic startle response[47,49]. In rodents, mGluRs have been implicated in various forms of the startle response, including regulation of paired-pulse inhibition by group II mGluRs, using pharmacological manipulation[50]. Recently, it has been shown that group II mGluRs are expressed across all main subdivisions

of the zebrafish brain[51]. Indeed, we found that conventional agonism of group II mGluRs by L-CCG-1 lowers the zebrafish ASR threshold.

The ability to target light to a subregion of the nervous system allowed us to localize the mGluR2-mediated effect on the acoustic startle response to the spinal cord and hindbrain and to find that optical activation of LimGluR2 also reduces acoustic startle response threshold, but, unlike L-CCG-1, this effect can be shown to result from acute activation of mGluR2 and can be reversed and repeated, suggesting that mGluR2 signaling could dynamically modulate escape threshold. Such information regarding the temporal dynamics of the acoustic startle response would not be possible to obtain using pharmacological approaches that require complete wash-out of ligands or addition of compounds whose activities are constrained by the pharmacokinetics of intact animals.

As with other GPCRs, mGluRs that couple to the same G-protein often activate distinct effectors[5] and are regulated distinctly[3,7]. Photo-agonism and photo-antagonism of group II and III mGluRs should make it possible to determine the precise spatial (i.e. pre vs. post-synaptic; synaptic vs. peri-synaptic vs. astrocytic) and temporal properties of signaling by individual receptors to mediate lasting changes in synaptic strength. Furthermore, since LimGluR2 maintains close to native ligand sensitivity, knock-in mice with a single point mutation to introduce a single cysteine anchor should allow for high resolution, specific photo-agonism or photo-antagonism while maintaining the receptor's native function. This would provide a new way to specifically probe the receptor's function in synaptic plasticity and learning, but also in anxiety, depression, and schizophrenia, for which they are major drug targets[33].

Online Methods

Chemical Synthesis

The chemical synthesis of D-MAG-0, D-MAG-1 and D-tether models was carried out as described in the Supplementary Information.

Homology Modeling and Monte Carlo Simulations

Homology modeling was performed using ProMod II in the Swiss Model environment[52]. The target sequence was the rat mGluR2 ligand binding domain (residues 23–538; Uniprot ID P31421) and the template was the open, glutamate-bound chain B of the rat mGluR1 structure (PDB ID IEWK) or the closed, glutamate-bound chain A of the rat mGluR3 structured (PDB ID 2E4U). Energy minimization was performed using the Gromos96 force field in DeepView (Swiss PDB Viewer).

Models of MAG were built in Maestro 6.5 (Schrödinger) starting with the experimental structures of *cis*-and *trans*-azobenzene[35]. The MCMM search[36] (Macromodel 9.1, Schrödinger) considered all dihedral angles as degrees of freedom with the exception of those in glutamate and azobenzene. Solvent was treated implicitly using a generalized Born/surface area water model in the context of the OPLS-2005 force field[53]. Bond lengths, bond angles and dihedral angles of azobenzene were constrained to the experimental structures. Protein sidechains were allowed to fluctuate while backbone atoms were frozen. After the

simulation, all structures were exported from Maestro, checked for steric clashes using the command line version of MolProbity[54] and imported into Igor Pro (Wavemetrics). The distance of the Mal-group to all residues was measured for every structure and for each residue the number of structures with distances less than 6.5Å was counted. Figures were made using PyMOL.

Molecular Biology and Gene Expression in Cultured Cells

Cysteine mutations were introduced into mGluR2, mGluR3, and mGluR6 cDNA in the pCDNA3.1 expression vector (CMV promoter) using the QuickChange mutagenesis kit (Agilent). GIRK1 (with F137S homotetramerization mutation[55]), eYFP, and RO4 were also inserted into pcDNA3.1. HEK293 and HEK293T cells were transiently cotransfected using Lipofectamine 2000 (Invitrogen) with mGluR mutants, GIRK1-F137S (homotetramerization mutant) and eYFP at a ratio of 7.5:7.5:1 with 1.6 μg of DNA total per 18 mm cover slip. RO4-transfected cells were maintained in dark room conditions. Cultured hippocampal neurons were transfected using the calcium phosphate method. Each coverslip received 1.1 μg of mGluR2-L300C DNA (or S302C) and 0.2 μg of eGFP DNA or 1.3 μg of mGluR2-L300C-GFP. mGluR2-L300C and mGluR2-S302C were inserted into a plasmid under the control of a synapsin promoter (pcDNA3.1 with the human synapsin promoter) to target expression to neurons.

Cultured Cell Electrophysiology

HEK293 cells were maintained in DMEM with 5% FBS on poly-L-lysine-coated glass coverslips. Dissociated hippocampal neurons were obtained from postnatal rats (P0-1) and plated at 75,000 cells/coverslip on poly-L-lysine-coated glass coverslips (12 mM). For autapse experiments low density cultures of 25,000 cells/coverslip were used. Neurons were maintained in media containing MEM supplemented with 5% fetal bovine serum, B27 (Invitrogen), and GlutaMAX (Invitrogen).

HEK293 and 293T whole cell patch clamp electrophysiology was performed 24–48 h after transfection in high potassium (HK) solution containing (in mM): 60 KCl, 89 NaCl, 1 $MgCl_2$, 2 $CaCl_2$, 10 Hepes, pH 7.4. Glass pipettes of resistance between 3 and 6 MΩ were filled with intracellular solution containing (in mM): 140 KCl, 10 Hepes, 3 Na_2ATP, 0.2 Na_2GTP, 5 EGTA, 3 $MgCl_2$, pH 7.4. Cells were voltage clamped to −60 to −80 mV using an Axopatch 200A (Molecular Devices) amplifier.

Hippocampal neuron whole cell patch clamp electrophysiology was performed 3–6 days after transfection (DIV 12–15). For voltage clamp recordings a high potassium extracellular solution containing (in mM): 79.5 NaCl, 60 KCl, 1.2 $MgCl_2$, 2.5 $CaCl_2$, 10 glucose, 5 Hepes, pH 7.4 was used. For all other experiments, extracellular solution contained (in mM): 138 NaCl, 1.5 KCl, 1.2 $MgCl_2$, 2.5 $CaCl_2$, 10 glucose, 5 Hepes, pH 7.4. Intracellular solution contained (in mM): 140 K-Gluconate, 10 NaCl, 5 EGTA, 2 $MgCl_2$, 1 CaCl2, 10 Hepes, 2 MgATP, 0.3 Na_2GTP, pH 7.2. For current step experiments, cells were adjusted to −50 mV with current injection before current steps were initiated to normalize spike count comparisons between cells. Only cells with a resting potential ≤−45 mV were analyzed. For autapse experiments, cells were voltage clamped to −70 and stepped to 0 mV for 2 ms. Post-

synaptic currents were delayed by 3 ms which confirmed autaptic origins of transmission. Inter-stimulus intervals were >12 s. EPSCs and IPSCs were identified based on the kinetics of decay with EPSCs approximately ten times faster than IPSCs (~5ms vs. 50 ms), as has been described previously[56]. All pharmacological compounds were obtained from Tocris and dissolved in extracellular buffers before application using a gravity-driven perfusion system.

For most experiments, illumination was applied to the entire field of view using a Polychrome V monochromator (TILL Photonics) through a 20x objective or a Lambda DG4 high speed wavelength switcher (Sutter Instruments) with 380 nm and 500 nm filters through a 40x objective. For bistable switching the DG-4 was coupled to the microscope through a 40x objective. Ultrafast, sub-millisecond photo-switching was achieved using a laser spot illumination system, for which the output of a 375/488 nm dual laser diode module (Omicron LDM) was coupled into a multi-mode fiber (10 μm, NA 0.1). The light exiting from this fiber was collimated and directed to the back aperture of the objective (Olympus 40x, NA 0.6). Intensities in the sample plane were >40 W/mm^2.

pClamp software was used for both data acquisition and control of illumination. To conjugate MAG, cells were incubated in 50–100 μM MAG for 30–60 minutes in the dark at room temperature in standard extracellular cell buffers.

For RO4 experiments cells were labeled with 1 μM 11-cis retinal for 40 minutes and experiments were performed under dark room conditions.

cAMP Measurements

Intracellular cAMP levels were assayed with an ELISA system from Applied Biosystems (Bedford, MA). HEK 293T cells grown to confluence on a 24-well plate were either exposed to D-MAG-0 (50 μM for 45 minutes in standard extracellular buffer) or to a similar volume of standard extracellular buffer. After washing (5x, 1 ml), cells were treated with forskolin and/or glutamate or 365 nm light and disrupted in lysis buffer 10 minutes later. For D-MAG-0 labeled cells, 365 nm illumination was controlled with a handheld lamp and applied for 10 s immediately after forskolin addition. Serial dilutions of cAMP served as standards. Samples of cell lysate and standards were incubated with anti-cAMP antibody and cAMP-AP in a 96-well plate. Then the plate was washed, incubated with substrate and finally chemiluminesence generated at the end of enzymatic reaction were measured in a luminometer, LmaxII 384 (Molecular Devices, Sunnyvale, CA).

Hippocampal Slice Gene Expression and Electrophysiology

Hippocampi were obtained from postnatal Sprague-Dawley rats (p. 7) and 400 μM slices were prepared and cultured as previously described[38]. After 3 days, slices were transfected by Biolistic gene transfer using a BioRad Helios Gene Gun and gold microcarriers coated with both mGluR2-L300C and tdTomato DNA.

Patch clamp recordings were obtained after 6–9 d *in vitro*. Before recording, slices were incubated at 32 °C for 40 min with D-MAG-0 (50 μM) diluted in NMDG-labeling solution containing (in mM): 150 NMDG-HCl, 3 KCl, 0.5 $CaCl_2$, 5 $MgCl_2$, 10 HEPES and 5

glucose, pH 7.4). Whole-cell patch-clamp recordings were performed on an upright Zeiss AxioExaminer using an Axopatch 200B amplifier (Molecular Devices). Pipettes of resistances 3–7 MΩ were filled with solution containing (in mM) 120 potassium-gluconate, 8 NaCl, 10 HEPES, 2 $MgCl_2$, 2 MgATP, 0.3 NaGTP and 10 EGTA, pH 7.4. aCSF containing (in mM) 119 NaCl, 2.5 KCl, 1.3 $MgSO_4$, 1 NaH_2PO_4-H_2O, 26.2 $NaHCO_3$, 11 glucose and 2.5 $CaCl_2$ was continuously perfused and bubbled with 95% O_2/5% CO_2. A DG-4 (Sutter Instruments) was coupled to the microscope for photoswitching through a 40× objective. Light intensity was approximately 20 mW mm^{-2} at 390 nm and 40 mW mm^{-2} at 500 nm.

Zebrafish Transgenesis

Expression of mGluR2-L300C was targeted to neurons using the UAS/GAL4 system. The transgenesis *UAS:LimGluR2(L300C)/cry:CER* construct contains the LimGluR2(L300C) ORF amplified from the expression vector pcDNA3.1. LimGluR2 expression is driven by an upstream sequence composed of 10X UAS repeats followed by the adenovirus E1b TATA box and a 5′ UTR from carp b-actin. The UAS sequence was amplified from the p5E-UAS vector, tol2 Kit[57]. The opposite strand contains a crystalline promoter sequence[58] driving expression of the ceruleam fluorescent protein in the crystalline of the eye for easy screening of transgenic fish. The expression sequences are flanked by sites for the fish transgenesis system meganuclease Isce-1[59].

Wild-type AB embryos were injected at the one-cell stage with 30 ng/ml *UAS:LimGluR2(L300C)/cry:CER DNA*, 10 units I-Sce1 (New England Biolabs R0694L), NEBuffer Isce-1 0.5X, and 0.1% Phenol Red. F1 embryos were raised and screened at 3dpf by fluorescence microscopy for presence of ceruleam fluorescent protein expression in the eye. F0 founder fish that generated *UAS:LimGluR2(L300C)/cry:CER* positive F1 fish were crossed to wild-type fish to create stable lines. *UAS:LimGluR2(L300C)/cry:CER* fish were crossed to HuC:Gal4;UAS:Kaede (gift from Baier Lab, UCSF) fish to generate *HuC:Gal4; UAS:Kaede; UAS:LimGluR2/cry:CER* fish in which Gal4 drives pan-neuronal expression of the Kaede fluorescent protein and LimGluR2(L300C).

Zebrafish Behavioral Assay

D-MAG-0 was diluted to 50 μM in 1 ml of a 5% DMSO Ringer buffered solution (in mm: 116 NaCl, 2.9 KCl, 1.8 CaCl2, 5 Hepes, pH 7.2), and pre-illuminated with UV light (365 nm) for 45 seconds. The labeling solution was added to 5dpf larvae (20–30 fish). The larvae were kept at 28.5°C in the dark for 45 minutes. Next, the larvae were washed in fish medium E3 and kept in the presence of E3 in the dark for a recovery period of 1h at 28.5°C. Control fish were subjected to the same protocol, but in the absence of D-MAG-0. For pharmacological experiments L-CCG-1 (Tocris) was diluted in E3 solution to a final concentration of 20 μM. Experimental and control fish were kept overnight at 28.5°C before mounting and testing for ASR.

Larvae were mounted in a glass well petri dish dorsal side up in 2% agar E3 solution at 36°C. Agar was removed from a region caudal to the fish otic vesicle. All experimental larvae used in experiments had an intact ASR, as determined by a light tap in the dish

containing the larvae. Tail-free mounted fish were attached with adhesive tape to the surface of an 8-Ohm mini-speaker (Radioshack, #273- 092). Fish were illuminated from the side with attenuated white light. Images were captured at 30Hz by a behavioral camera (IDS, USB 2 uEye). A square wave, (900Hz, 120ms, controllable amplitude) stimulus was generated by a function waveform generator (Agilent, 33220A) connected to the mini-speaker. Sound/vibration-induced escapes were determined by observation in behavioral movies of characteristic C-bends induced by sound/vibration stimulus. Threshold was defined as the minimum energy capable of inducing >50% C-bends in a 10 trial test. All experiments were performed in a climate-controlled environment at 22°C.

The illumination source was a Lambda DG4 high-speed wavelength switcher (Sutter). A digital micro-mirror device was used to pattern illumination through a 2.5X Zeiss objective. Illumination reached the larvae from the dorsal side and covered a region caudal to the eyes and reaching almost the whole length of the spinal cord. Activation and deactivation wavelengths were 380/15nm, 0.09 mW/mm2 for 400ms, and 510/20nm, 0.49 mW/mm2 for 1 second. Larvae were sound/vibration-stimulated 5 seconds after illumination. 10 stimuli with a 10s inter-stimulus interval were performed for each condition. Illumination and behavioral set up were mounted on a 3i Marianas system with a spinning disk confocal (Yokagawa) mounted on a Zeiss microscope.

For the L-CCG-1 experiment, 5–6 dpf WT zebrafish larvae were treated overnight in 20 μM LCCG-1- or vehicle-containing E3 solution. Trials were performed with a 10 second ISI and speaker voltage was increased in steps of 500 mVpp until the threshold was reached. All fish had an intact ASR as determined by a light tap to the dish.

For swimming and escape response control experiments, zebrafish larvae were kept in E3 in 48-well microplates mounted on a plexiglass box. For fish activity measurements, an infrared CCD camera (fire-i 780b, Unibrain) from above was used with trans-infrared illumination from below (see Fig. S10a,b). Sound stimuli were administered by two speakers (Visaton SC 5.9) screwed to the same plexiglass plate as the micro-well plate. Stimuli (powered by a 15W amplifier) were sent to speakers using a Native Instruments PCI-6229 DAQ controlled by Matlab. Duration and frequency were 20ms and 900Hz, respectively. Escapes were detected using an in-house movement threshold algorithm. The acoustic stimulus was applied 110ms after start of the movie. A successful escape response was counted if the difference of the integrated pixel values of the two frames immediately after the stimulus was statistically higher ($P < 0.01$) than the distribution of pixel-change values in the preceding 109 frames of recorded spontaneous activity. The accuracy of this algorithm was verified by visual inspection of movies.

Animal experiments were done under oversight by the University of California institutional review board (Animal Care and Use Committee).

Statistics and Data Analysis

Data was analyzed using Clampfit (Axon Instruments) and Origin (OriginLab) software. Statistical analysis was performed using Microsoft Excel. All values reported are mean ± s.e.m.

Supplementary Material

Refer to Web version on PubMed Central for supplementary material.

Acknowledgments

We thank Andrew P. Mariani for 11-*cis* retinal, J.P. Pin for the mGluR plasmids and E. Reuveny for the GIRK1 plasmid; K. Durkin, K. Dubay, T. Berger, G. Sandoz, S. Berlin for helpful discussion; A. Guyon, Z. Fu, and S. Szobota for help with slice cultures; Z. Fu for molecular biology assistance; K. McDaniel, J. Maxfield, J. Saint-Hillaire, and D. Weinman for fish care; E. Carroll for discussion and help with zebrafish set up; Philipp Gut (UCSF) for zebrafish plasmids; Herwig Baier (UCSF) for fish lines; and the College of Chemistry (UC Berkeley) for computing resources for the Monte Carlo simulations. Support for the work was provided by the Nanomedicine Development Center for the Optical Control of Biological Function, NIH PN2EY018241 (D.T. & E.Y.I.), the Human Frontier Science Program, RGP0013/2010 (E.Y.I.), the Deutsche Forschungsgemeinschaft (SFB 879, D.T.), the Fond der Chemischen Industrie (Kekulé fellowship to P.S.), NSF CHE-0233882 and CHE-0840505 (to the UC Berkeley College of Chemistry), a postdoctoral fellowship of the European Molecular Biology Organization (H.J.) and a predoctoral fellowship from the Fulbright Foundation (B.G.).

References

1. Szobota S, Isacoff EY. Optical control of neuronal activity. Annu Rev Biophys. 2010; 39:329–48. [PubMed: 20192766]
2. Deisseroth K. Optogenetics. Nat Methods. 2011; 8:26–9. [PubMed: 21191368]
3. Pierce KL, Premont RT, Lefkowitz RJ. Seven-transmembrane receptors. Nat Rev Mol Cell Biol. 2002; 3:639–50. [PubMed: 12209124]
4. Kobilka BK. Structural insights into adrenergic receptor function and pharmacology. Trends Pharmacol Sci. 2011; 32:213–8. [PubMed: 21414670]
5. Niswender CM, Conn PJ. Metabotropic glutamate receptors: physiology, pharmacology, and disease. Annu Rev Pharmacol Toxicol. 2010; 50:295–322. [PubMed: 20055706]
6. Bockaert J, Perroy J, Becamel C, Marin P, Fagni L. GPCR interacting proteins (GIPs) in the nervous system: Roles in physiology and pathologies. Annu Rev Pharmacol Toxicol. 2010; 50:89–109. [PubMed: 20055699]
7. Gainetdinov RR, Premont RT, Bohn LM, Lefkowitz RJ, Caron MG. Desensitization of G protein-coupled receptors and neuronal functions. Annu Rev Neurosci. 2004; 27:107–44. [PubMed: 15217328]
8. Pei Y, Rogan SC, Yan F, Roth BL. Engineered GPCRs as tools to modulate signal transduction. Physiology (Bethesda). 2008; 23:313–21. [PubMed: 19074739]
9. Alexander GM, et al. Remote control of neuronal activity in transgenic mice expressing evolved G protein-coupled receptors. Neuron. 2009; 63:27–39. [PubMed: 19607790]
10. Yamashita T, Terakita A, Shichida Y. Distinct roles of the second and third cytoplasmic loops of bovine rhodopsin in G protein activation. J Biol Chem. 2000; 275:34272–9. [PubMed: 10930404]
11. Yamashita T, Terakita A, Shichida Y. The second cytoplasmic loop of metabotropic glutamate receptor functions at the third loop position of rhodopsin. J Biochem. 2001; 130:149–55. [PubMed: 11432791]
12. Zemelman BV, Lee GA, Ng M, Miesenbock G. Selective photostimulation of genetically chARGed neurons. Neuron. 2002; 33:15–22. [PubMed: 11779476]
13. Li X, et al. Fast noninvasive activation and inhibition of neural and network activity by vertebrate rhodopsin and green algae channelrhodopsin. Proc Natl Acad Sci U S A. 2005; 102:17816–21. [PubMed: 16306259]
14. Gutierrez DV, et al. Optogenetic control of motor coordination by Gi/o protein-coupled vertebrate rhodopsin in cerebellar Purkinje cells. J Biol Chem. 2011; 286:25848–58. [PubMed: 21628464]
15. Melyan Z, Tarttelin EE, Bellingham J, Lucas RJ, Hankins MW. Addition of human melanopsin renders mammalian cells photoresponsive. Nature. 2005; 433:741–5. [PubMed: 15674244]
16. Qiu X, et al. Induction of photosensitivity by heterologous expression of melanopsin. Nature. 2005; 433:745–9. [PubMed: 15674243]

17. Lin B, Koizumi A, Tanaka N, Panda S, Masland RH. Restoration of visual function in retinal degeneration mice by ectopic expression of melanopsin. Proc Natl Acad Sci U S A. 2008; 105:16009–14. [PubMed: 18836071]
18. Kim JM, et al. Light-driven activation of beta 2-adrenergic receptor signaling by a chimeric rhodopsin containing the beta 2-adrenergic receptor cytoplasmic loops. Biochemistry. 2005; 44:2284–92. [PubMed: 15709741]
19. Airan RD, Thompson KR, Fenno LE, Bernstein H, Deisseroth K. Temporally precise in vivo control of intracellular signalling. Nature. 2009; 458:1025–9. [PubMed: 19295515]
20. Oh E, Maejima T, Liu C, Deneris E, Herlitze S. Substitution of 5-HT1A receptor signaling by a light-activated G protein-coupled receptor. J Biol Chem. 2010; 285:30825–36. [PubMed: 20643652]
21. Bailes HJ, Zhuang LY, Lucas RJ. Reproducible and sustained regulation of Galphas signalling using a metazoan opsin as an optogenetic tool. PLoS One. 2012; 7:e30774. [PubMed: 22292038]
22. Fehrentz T, Schonberger M, Trauner D. Optochemical genetics. Angew Chem Int Ed Engl. 2011; 50:12156–82. [PubMed: 22109984]
23. Banghart M, Borges K, Isacoff E, Trauner D, Kramer RH. Light-activated ion channels for remote control of neuronal firing. Nat Neurosci. 2004; 7:1381–6. [PubMed: 15558062]
24. Volgraf M, et al. Allosteric control of an ionotropic glutamate receptor with an optical switch. Nat Chem Biol. 2006; 2:47–52. [PubMed: 16408092]
25. Anwyl R. Metabotropic glutamate receptor-dependent long-term potentiation. Neuropharmacology. 2009; 56:735–40. [PubMed: 19705571]
26. Luscher C, Huber KM. Group 1 mGluR-dependent synaptic long-term depression: mechanisms and implications for circuitry and disease. Neuron. 2010; 65:445–59. [PubMed: 20188650]
27. Panatier A, et al. Astrocytes are endogenous regulators of basal transmission at central synapses. Cell. 2011; 146:785–98. [PubMed: 21855979]
28. Bradley SJ, Challiss RA. G protein-coupled receptor signalling in astrocytes in health and disease: A focus on metabotropic glutamate receptors. Biochem Pharmacol. 2012
29. Tanabe Y, Masu M, Ishii T, Shigemoto R, Nakanishi S. A family of metabotropic glutamate receptors. Neuron. 1992; 8:169–79. [PubMed: 1309649]
30. Saugstad JA, Segerson TP, Westbrook GL. Metabotropic glutamate receptors activate G-protein-coupled inwardly rectifying potassium channels in Xenopus oocytes. J Neurosci. 1996; 16:5979–85. [PubMed: 8815880]
31. Ikeda SR, Lovinger DM, McCool BA, Lewis DL. Heterologous expression of metabotropic glutamate receptors in adult rat sympathetic neurons: subtype-specific coupling to ion channels. Neuron. 1995; 14:1029–38. [PubMed: 7538309]
32. Altinbilek B, Manahan-Vaughan D. A specific role for group II metabotropic glutamate receptors in hippocampal long-term depression and spatial memory. Neuroscience. 2009; 158:149–58. [PubMed: 18722513]
33. Marek GJ. Metabotropic glutamate 2/3 receptors as drug targets. Curr Opin Pharmacol. 2004; 4:18–22. [PubMed: 15018834]
34. Muto T, Tsuchiya D, Morikawa K, Jingami H. Structures of the extracellular regions of the group II/III metabotropic glutamate receptors. Proc Natl Acad Sci U S A. 2007; 104:3759–64. [PubMed: 17360426]
35. Tsuji T, Takashima H, Takeuchi H, Egawa T, Konaka S. Molecular structure and torsional potential of trans-azobenzene. A gas electron diffraction study. Journal of Physical Chemistry A. 2001; 105:9347–9353.
36. Chang G, Guida WC, Still WC. An Internal Coordinate Monte-Carlo Method for Searching Conformational Space. Journal of the American Chemical Society. 1989; 111:4379–4386.
37. Gorostiza P, et al. Mechanisms of photoswitch conjugation and light activation of an ionotropic glutamate receptor. Proc Natl Acad Sci U S A. 2007; 104:10865–70. [PubMed: 17578923]
38. Janovjak H, Szobota S, Wyart C, Trauner D, Isacoff EY. A light-gated, potassium-selective glutamate receptor for the optical inhibition of neuronal firing. Nat Neurosci. 2010; 13:1027–32. [PubMed: 20581843]

39. Iacovelli L, et al. Regulation of group II metabotropic glutamate receptors by G protein-coupled receptor kinases: mGlu2 receptors are resistant to homologous desensitization. Mol Pharmacol. 2009; 75:991–1003. [PubMed: 19164443]
40. Raveh A, Cooper A, Guy-David L, Reuveny E. Nonenzymatic rapid control of GIRK channel function by a G protein-coupled receptor kinase. Cell. 2010; 143:750–60. [PubMed: 21111235]
41. Hanna L, et al. Differentiating the roles of mGlu2 and mGlu3 receptors using LY541850, an mGlu2 agonist/mGlu3 antagonist. Neuropharmacology. 2013; 66:114–21. [PubMed: 22445601]
42. Ehrengruber MU, et al. Activation of heteromeric G protein-gated inward rectifier K+ channels overexpressed by adenovirus gene transfer inhibits the excitability of hippocampal neurons. Proc Natl Acad Sci U S A. 1997; 94:7070–5. [PubMed: 9192693]
43. Takahashi T, Forsythe ID, Tsujimoto T, Barnes-Davies M, Onodera K. Presynaptic calcium current modulation by a metabotropic glutamate receptor. Science. 1996; 274:594–7. [PubMed: 8849448]
44. Shigemoto R, et al. Differential presynaptic localization of metabotropic glutamate receptor subtypes in the rat hippocampus. J Neurosci. 1997; 17:7503–22. [PubMed: 9295396]
45. Leaney JL. Contribution of Kir3.1, Kir3.2A and Kir3.2C subunits to native G protein-gated inwardly rectifying potassium currents in cultured hippocampal neurons. Eur J Neurosci. 2003; 18:2110–8. [PubMed: 14622172]
46. Koch M. The neurobiology of startle. Prog Neurobiol. 1999; 59:107–28. [PubMed: 10463792]
47. Burgess HA, Granato M. Sensorimotor gating in larval zebrafish. J Neurosci. 2007; 27:4984–94. [PubMed: 17475807]
48. Caporale N, et al. LiGluR restores visual responses in rodent models of inherited blindness. Mol Ther. 2011; 19:1212–9. [PubMed: 21610698]
49. Korn H, Faber DS. The Mauthner cell half a century later: a neurobiological model for decision-making? Neuron. 2005; 47:13–28. [PubMed: 15996545]
50. Grauer SM, Marquis KL. Intracerebral administration of metabotropic glutamate receptor agonists disrupts prepulse inhibition of acoustic startle in Sprague-Dawley rats. Psychopharmacology (Berl). 1999; 141:405–12. [PubMed: 10090648]
51. Haug MF, Gesemann M, Mueller T, Neuhauss SC. Phylogeny and expression divergence of metabotropic glutamate receptor genes in the brain of zebrafish (Danio rerio). J Comp Neurol. 2012
52. Bordoli L, et al. Protein structure homology modeling using SWISS-MODEL workspace. Nat Protoc. 2009; 4:1–13. [PubMed: 19131951]
53. Kaminski GA, Friesner RA, Tirado-Rives J, Jorgensen WL. Evaluation and reparametrization of the OPLS-AA force field for proteins via comparison with accurate quantum chemical calculations on peptides. Journal of Physical Chemistry B. 2001; 105:6474–6487.
54. Davis IW, et al. MolProbity: all-atom contacts and structure validation for proteins and nucleic acids. Nucleic Acids Res. 2007; 35:W375–83. [PubMed: 17452350]
55. Vivaudou M, et al. Probing the G-protein regulation of GIRK1 and GIRK4, the two subunits of the KACh channel, using functional homomeric mutants. J Biol Chem. 1997; 272:31553–60. [PubMed: 9395492]
56. Bekkers JM, Stevens CF. Excitatory and inhibitory autaptic currents in isolated hippocampal neurons maintained in cell culture. Proc Natl Acad Sci U S A. 1991; 88:7834–8. [PubMed: 1679238]
57. Kwan KM, et al. The Tol2kit: a multisite gateway-based construction kit for Tol2 transposon transgenesis constructs. Dev Dyn. 2007; 236:3088–99. [PubMed: 17937395]
58. Kurita R, et al. Suppression of lens growth by alphaA-crystallin promoter-driven expression of diphtheria toxin results in disruption of retinal cell organization in zebrafish. Dev Biol. 2003; 255:113–27. [PubMed: 12618137]
59. Grabher C, Wittbrodt J. Meganuclease and transposon mediated transgenesis in medaka. Genome Biol. 2007; 8 (Suppl 1):S10. [PubMed: 18047687]

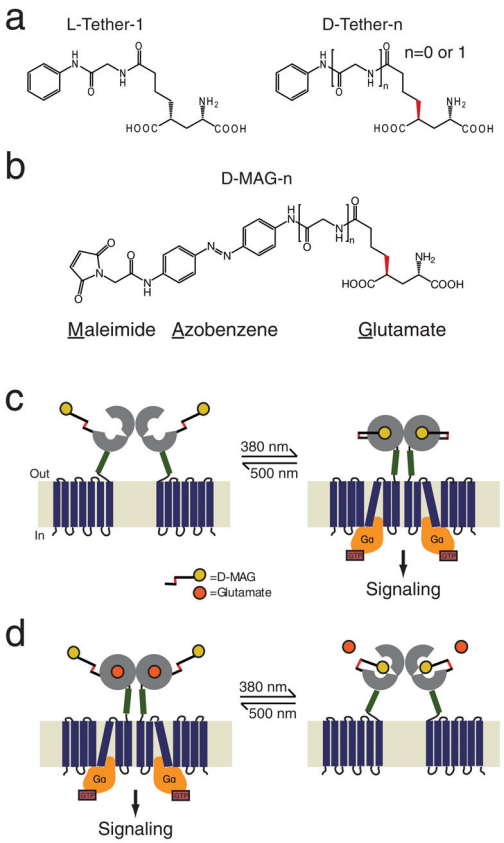

Figure 1.

Design of photoswitches for light-control of mGluR2. (**a)** Chemical structure of tether models including previously described L-Tether-1 and new 4-D versions with two different linker lengths (D-Tether-0 and D-Tether-1) **(b)** Structure of D-MAG molecules. 380 nm light maximally isomerizes to the *cis* state, whereas 500 nm light isomerizes to the *trans* state. Spontaneous thermal relaxation from *cis* to *trans* occurs over tens of minutes at room temperature. **(c)** Schematic view of light-induced agonism. mGluRs contain a ligand-binding clamshell domain (LBD; grey) that is coupled to a 7-transmembrane domain (TMD; green) by a cysteine rich domain (CRD, dark blue). Agonist binding to the LBD initiates clamshell closure, which rearranges a dimer interface with a partner LBD of a second subunit and transmits a conformational change via the TMD to the cytoplasmic domain, thereby activating G-proteins. Under 380 nm illumination D-MAG enters the *cis* state and reorients the glutamate moiety into the ligand binding site to drive clamshell closure and activate G protein and downstream signaling. **(d)** Schematic of 380 nm-induced antagonism. Glutamate (dark orange circles) is shown in the bound, activated state of mGluR2. Upon photoisomerization the glutamate end of MAG enters the binding site and prevents clamshell closure, thus deactivating the receptor.

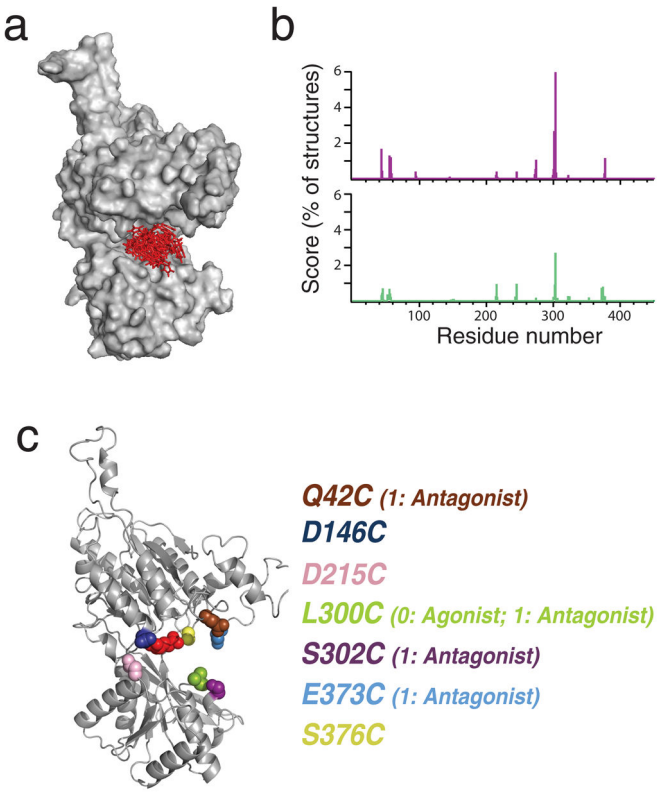

Figure 2.

Monte Carlo simulations and cysteine-scanning of mGluR2 ligand-binding domain. **(a)** *cis*-D-MAG-0 (red stick depiction) with glutamate end bound in LBD (gray surface depiction) is shown in 20 superposed conformations calculated by Monte Carlo simulation using homology model of the mGluR2 LBD in the open, glutamate-bound conformation. **(b)** Results of D-MAG-0 simulations for *cis* and *trans* conformations. Lines indicate the frequency with which the maleimide end of MAG approaches within 6Å of the Cα of a particular residue in the *cis* state (purple) and *trans* state (green). **(c)** Open homology model of mGluR2 LBD showing native side chains of 7 residues individually substituted to cysteine. Results of photoswitching of D-MAG-0 and D-MAG-1 attached at each of the positions where any photoresponse was observed are shown in parentheses. “0” indicates D-MAG-0 and “1” indicates D-MAG-1. Data from ≥2 different coverslips for all conditions tested.

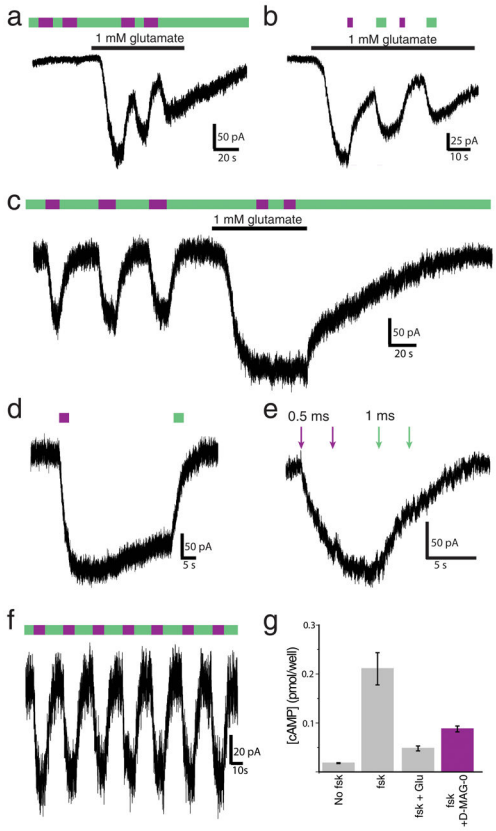

Figure 3.

Photo-antagonism and photo-agonism of mGluR2. **(a–f)** Effects of photoswitching D-MAG0 and D-MAG1 on the activation of GIRK1 current in HEK293 cells. **(a)** When D-MAG-1 is attached to S302C ("LimGluR2-block") light has no effect in the absence of glutamate, but 380 nm light evokes photo-antagonism in the presence of glutamate. Black bars indicate application of 1 mM L-glutamate. Green bars indicate illumination with 500 nm light and purple bars indicate 380 nm light. **(b)** LimGluR2-block photo-antagonism is bistable. A brief flash of 380 nm induces a decrease in glutamate-evoked current which is sustainted in the dark until it is reversed by 500 nm. **(c)** When D-MAG-0 is attached to L300C 380 nm light evokes GIRK1 current on its own. The current remains activated until deactivation is initiated by 500 nm light. No photo-antagonism is seen in the presence of glutamate, indicating that D-MAG-0 is not a partial agonist of mGluR2- L300C. **(d)** LimGluR2-mediated GIRK1 current shows sustained response in the dark following a brief illumination at 380. **(e)** At higher light intensities (~40 W/mm^2), 0.5 ms 380 nm pulses can activate and 1 ms 500 nm pulses can fully deactivate LimGluR2. The second 380 nm pulse shows minor further activation, indicating that the first pulse almost completely activated the receptors. **(f)** GIRK1 current evoked by repetitive rounds of photo-activation and photo-deactivation of mGluR2-L300C-D-MAG-0 ("LimGluR2") by pulses of 380 nm and 500 nm light, respectively. **(g)** LimGluR2 activation reduces cAMP elevation induced by a 10 minute application of 10 μM forskolin with similar to the efficacy to 1 mM glutamate application. Error bars show s.e.m. for n=3 coverslips per condition.

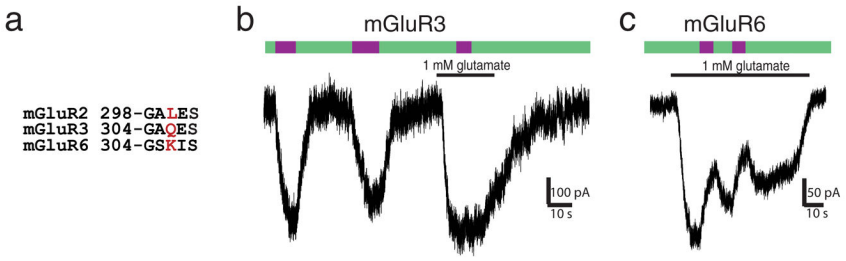

Figure 4.

Extension of photoswitching from mGluR2 to mGluR3 and mGluR6. **(a)** Local alignment of region containing D-MAG-0 anchoring sites in mGluR2 for LimGluR2 (red). **(b)** When D-MAG-0 is attached to mGluR3-Q306C ("LimGluR3") robust 380 nm-induced agonism is seen. Similar to LimGluR2, no photo-antagonism was seen in the presence of glutamate. **(c)** When D-MAG-0 is attached to mGluR6-K306C ("LimGluR6-block") robust 380 nm-induced photoantagonism is seen, indicating that the PTL approach can be extended to group III mGluRs.

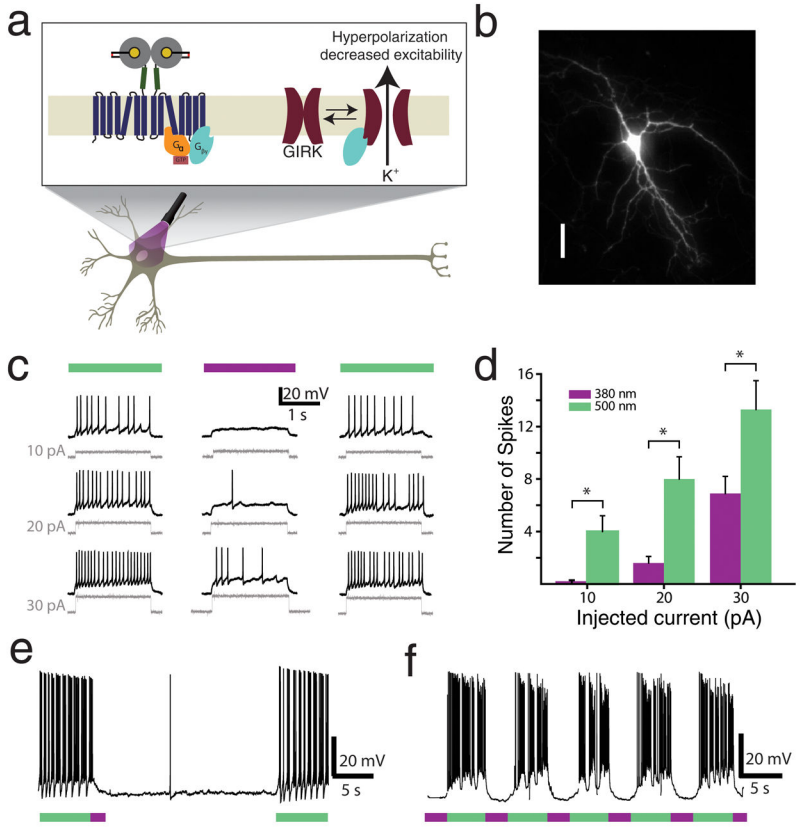

Figure 5.

LimGluR2 hyperpolarizes and reduces excitability in cultured hippocampal neurons. **(a)** Schematic showing LimGluR2 mediated control of excitability via GIRK channels. Note: Light is applied to entire field of view. **(b)** LimGluR2-eGFP is widely distributed in cultured hippocampal neuron. Scale = 50 μm. **(c)** Representative cell shows trains of spikes elicited by depolarizing current steps (gray traces) when LimGluR2 is off (500 nm illumination, green bar) are reversibly suppressed by activation of LimGluR2 (380 nm illumination, violet bar). (**d)** Summary of current step experiments shown in (C) for 8 cells. Bars indicate number of spikes in response to 2 s current injections under 380 nm (violet bar) or 500 nm (green bar) light and error bars indicate s.e.m. Star indicates statistical significance (paired, 1-tailed t-test, p=0.009, 0.004, and 0.009, respectively, for currents of 10, 20, and 30 pA; n=7 cells). (**e, f)** Representative cells show bistability and repeatability of LimGluR2. **(e)** LimGluR2-mediated hyperpolarization in representative cell in response to brief (1 s) activation by 380 nm light (violet bar) persists for tens of seconds in the dark before LimGluR2 deactivation by 500 nm light (green bar). The persistent activation in the dark effectively suppresses spikes**. (f)** Representative trace shows repeatable spike silencing by photocontrol of LimGluR2.

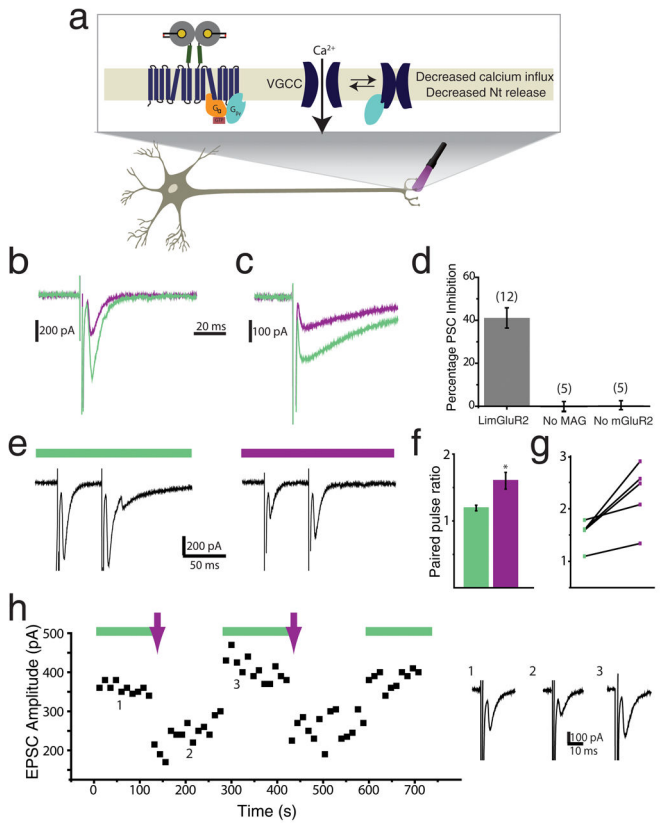

Figure 6.

Optical activation of LimGluR2 reversibly decreases excitatory and inhibitory postsynaptic currents and increases paired pulse facilitation at hippocampal autapses. **(a)** Schematic shows optical control of neurotransmitter release via LimGluR2 triggered G-protein suppression of opening of a presynaptic voltage-gated calcium channel (VGCC). **(b, c)** Representative autaptic excitatory (b) and inhibitory (c) postsynaptic currents elicited by short (2 ms) depolarizing steps are decreased in amplitude by LimGluR2 activation by 380 nm light (violet traces) compared to deactivation by 500 nm light (green traces. **(d)** Pooled inhibition of EPSCs and IPSCs by optical activation of LimGluR2 compared to controls in which mGluR2 (L300C) was expressed but not labeled with D-MAG-0 and where mGluR2 was not expressed. Values in parentheses denote number of cells tested and error bars show s.e.m. **(e)** Representative single sweeps of paired pulse recordings (50 ms inter-stimulus interval) of EPSCs under 500 nm light (green bar) followed by 380 nm light (violet bar). **(f)** Summary of paired pulse ratio (PPR) values for representative cell. 380 nm light (violet bar) significantly increased the PPR compared to 500 nm light (green bar) (n=10 sweeps/ condition; paired, 1-tailed t-test, p=0.008).Error bars show s.e.m.**(g)** Plot of average PPRs measured for 5 autaptic cells under 500 nm light (green symbols) and 380 nm light (violet symbols). **(h)** Representative EPSC amplitudes from a cell showing repeatable, bistable optical inhibition of an excitatory autapse. Illumination at 500 nm to deactivate LimGluR2 is followed by brief (1 s) illumination at 380 nm (violet arrows) followed by a period of darkness until illumination at 500 nm to deactivate LimGluR2 was resumed. Inserts (i), (ii), and (iii) show EPSCs from indicated times.

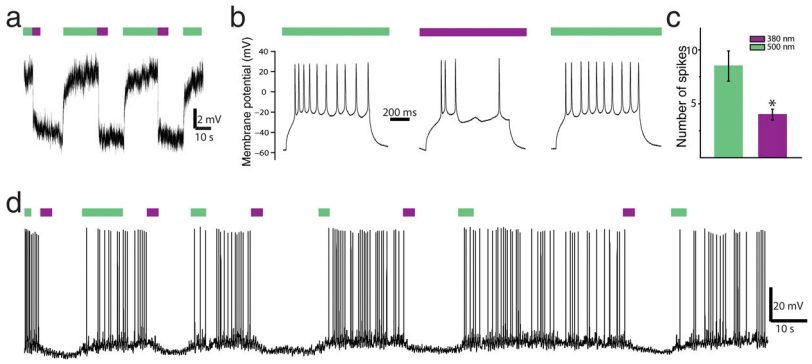

Figure 7.

LimGluR2-mediated control of neuronal excitability in hippocampal slice. **(a)** Hyperpolarization is triggered by illumination at 390 nm (violet bar) and reversed by illumination at 500 nm (green bar) in a representative cell. **(b)** Representative cell recorded in whole-cell patch in cultured hippocampal slice shows spike firing in response to 1s, 200 pA depolarizing current injections during 500 nm (green bars) or 380 nm (violet bar) illumination. LimGluR2 activation reversibly decreases the number of spikes. **(c)** Summary of optical control of spike firing in response to current steps in LimGluR2-positive neurons (n=6 cells). Star indicates statistical significance (paired, 1-tailed t-test, p=0.024) and error bars show s.e.m. **(e)** Representative trace showing reversible, bistable silencing of spontaneous activity by LimGluR2.

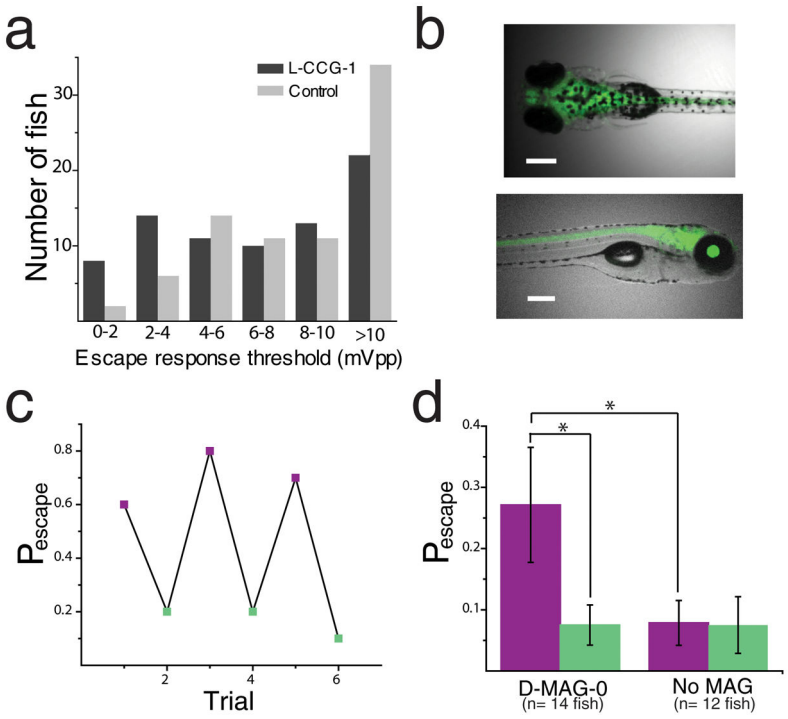

Figure 8.

Agonism of endogenous group II mGluRs and photo-agonism of LimGluR2 increases escape response probability in zebrafish larvae. **(a)** Treatment with the group II mGluR agonist L-CCG-1(10 μM) decreases the threshold of the WT zebrafish larvae ASR. The plot shows frequency distribution of minimum energy thresholds. Class >10 Vpp represent fish that had an intact ASR, but that did not respond with a C-bend at the highest sound energy attained by our experimental apparatus (10 Vpp). Comparison of the two groups was performed using the Mann-Whitney test, $z = 2.38$, $p < 0.02$, two tailed distribution. $n_{control} = n_{LCCG-1} = 78$ fish. **(b)** UAS-GFP imaging shows pan-neuronal expression in elavl3-GAL4 driver line. Scale=250 μm. **(c)** Representative larva showing reversible modulation of escape response probability. Each data point represents the escape probability during a period of ten trials. Violet and Green points represent trials after illumination at 510 and 380 nm, respectively. **(d)** Summary of LimGluR2-modulation of escape response. Green bars indicate illumination with 510 nm light and purple bars indicate 380 nm light. Stars indicate statistical significance (p=0.007 for comparison of 510 nm vs. 380 nm illumination for MAG-labeled larvae with 1-tailed paired T-Test and p=0.03 for comparison of MAG-labeled and unlabeled larvae with 1 tailed unpaired T-Test) and error bars show s.e.m.